Bonding study of TiC and TiN. I. High-precision x-ray-diffraction determination of the valence-electron density distribution, Debye-Waller temperature factors, and atomic static displacements in $TiC_{0.94}$ and $TiN_{0.99}$

A. Dunand, H. D. Flack, and K. Yvon
Laboratoire de Cristallographie aux Rayons X, Université de Genève, 24 quai Ernest Ansermet, CH-1211 Genève 4, Switzerland
(Received 29 February 1984)

Single-crystal, high-precision, high-resolution x-ray-diffraction measurements of the substoichiometric refractory compounds TiC and TiN have been performed with Ag$K\alpha$ radiation. Severe anisotropic general extinction affects the intense low-order reflections. Inhomogeneity in the mosaic spread and domain size produces small but significant differences between reflection and antireflection for the same plane of diffraction. These effects have been modeled and refined together with a scale factor, isotropic thermal parameters, a population parameter of the nonmetal site, the amplitude of metal-atom static displacements around nonmetal vacancies, and an atomic model which includes occupancy factors of the separate orbital contributions of the valence electrons combined with κ expansion-contraction parameters. At convergence, the "agreement indices" (or "reliability factors") were $R=0.0025$ for $TiC_{0.94}$ and $R=0.0023$ for $TiN_{0.99}$. The refined population parameters indicate a chemical composition of $TiC_{0.939(9)}$ and $TiN_{0.99(2)}$. The mean-square amplitudes of thermal vibrations, $\langle u^2\rangle_{Ti}=0.002\,38(2)$ Å^2, $\langle u^2\rangle_C=0.003\,35(8)$ Å^2, $\langle u^2\rangle_{Ti}=0.002\,94(1)$ Å^2, and $\langle u^2\rangle_N=0.003\,08(12)$ Å^2 are consistent with the respective atomic masses. 36% of the metal atoms in $TiC_{0.94}$ are involved in a relaxation around the nonmetal vacancies, being displaced from their sublattice sites by 0.097(2) Å along [100]. No evidence for static displacements was found in $TiN_{0.99}$. The valence-electron density distribution can be described satisfactorily in terms of deformed atoms. No buildup of charge density occurs between atomic sites. Our analysis, similar to a Mulliken partitioning, shows first that ionicity is important, with a charge transfer from the metal to the nonmetal of $[2.1(4)]e$ in the carbide and $[1.9(4)]e$ in the nitride, and secondly that the charge asphericity around the metal atoms is larger in the former than in the latter, while no departure from spherical symmetry is observed around the nonmetal atoms. The titanium $3d$ electrons can be split into a spherical shell that contains $[1.27(6)]e$ plus an excess of $[0.24(5)]e$ shared by two orbitals of e_g symmetry in the carbide and conversely into a spherical shell that contains $[0.88(11)]e$ plus an excess of $[0.12(9)]e$ shared by three orbitals of t_{2g} symmetry in the nitride. This suggests that the metal-to-metal bonding is similar in TiC and in TiN while the metal-to-nonmetal bonding is greater in TiC than in TiN.

I. INTRODUCTION

Titanium monocarbide and mononitride are hard, brittle refractory metallic solids (melting points at 3340 K for TiC and at 3222 K for TiN) (Ref. 1) which have sodium chloride structure. Owing to their unusual combination of properties, they have been extensively studied both experimentally[1] and theoretically.[2] An aspect which is of major interest but still incompletely understood is their bonding. Information on bonding may be obtained from, among other techniques, a valence-electron density distribution determination by x-ray diffraction.[3] TiC, TiN, and TiO—provided that well-characterized monocrystals are available—seem to be favorable compounds for such studies since they contain reasonably light elements and have a highly symmetric structure.

In the present paper (first of this series), the results of a high-precision, high-resolution [$(\sin\theta)/\lambda_{max}=1.73$ Å^{-1}] x-ray-diffraction study on crystals of composition $TiC_{0.94}$ and $TiN_{0.99}$ are presented. The experimental details are described in Sec. II. In Sec. III the data are analyzed in terms of an atomic model with partial orbital occupancies and radial expansion-contraction of the valence shells, with harmonic thermal vibrations and with partial metal-atom static displacements. The results are presented in Sec. IV both in the form of valence-electron density maps and as numerical values of the parameters describing the model. There are no published data in the literature giving either experimental electron density values or high-accuracy metal-atom static displacements in the compounds $TiC_{0.94}$ and $TiN_{0.99}$

In the following paper,[4] these valence-electron distributions will be compared to theoretical ones for defect-free crystals of TiC and TiN,[5] which have been derived from published data of self-consistent augmented-plane-wave (APW) band-structure calculations.[6]

II. EXPERIMENTAL DETAILS

A. Sample preparation

Well-defined single crystals of composition $TiC_{0.940(5)}$ and $TiN_{0.992(5)}$ were supplied by Dr. C. Politis

(Karlsruhe). The carbide was prepared by a hot-pressing and recrystallization technique at 3000 K and 20 $MN\,m^{-2}$,[7] whereas the nitride was obtained by chemical-vapor deposition in a Mo tube.[8] Their composition was determined by chemical analysis, and their impurity contents were stated to be $N \leq 100$ ppm and $O \leq 100$ ppm in $TiC_{0.94}$, and $C \leq 200$ ppm, and $O \leq 800$ ppm in $TiN_{0.99}$.[7]

Crystal fragments of irregular shape were ground in a diamond-coated compressed-air mill, yielding single crystals of almost spherical shape. While the $TiC_{0.94}$ crystal chosen resembled a rounded-off cube with minimum dimensions of 0.166(3) mm between two cube faces and maximum dimensions of 0.179(3) mm along the face diagonals, giving an average diameter of 0.176(5) mm, the $TiN_{0.99}$ crystal was a nearly perfect sphere of average diameter 0.209(3) mm. The quality of both crystals was tested by taking well-exposed x-ray Laue photographs (Cu anticathode). Sharp spots were observed, except for sickle-shaped areas of diffuse scattering in the vicinity of a few reflections which was assigned to the diffraction, at the characteristic wavelengths, from misaligned blocks of the damaged, abraded surface layer of the crystals. The lattice parameter of $TiC_{0.94}$ was determined from precise diffractometer measurements of the Bragg angles of reflections $\{666\}$ with $AgK\alpha_1$ [$\lambda = 0.559\,407\,5$ Å (Ref. 9)], and $\{751\}$ and $\{555\}$ with $MoK\alpha_1$ [$\lambda = 0.709\,300$ Å (Ref. 9)], whereas that of $TiN_{0.99}$ was determined from $\{10\,2\,2\}$ and $\{666\}$ using $AgK\alpha_1$ and $AgK\alpha_2$ [$\lambda = 0.563\,798$ Å (Ref. 9)] β-filtered radiations. The following values (only accurate to about 1 part in 10 000), with estimated standard deviations in parentheses, were found:

For $TiC_{0.94}$, $a = 4.329\,65(13)$ Å .

For $TiN_{0.99}$, $a = 4.241\,29(3)$ Å .

The unit-cell constant of the carbide is consistent with published values, $4.32 < a < 4.33$ Å, for $TiC_{0.94}$ (Ref. 10), and confirms the low nitrogen and oxygen content since significant amount of either impurity would lead to smaller lattice parameters. The constant of the nitride slightly exceeds that reported for vapor-deposited $TiN_{0.99}$ [$a = 4.2401(3)$ Å] (Ref. 8) and that derived from the lattice-parameter—nitrogen-content relation $a = 4.1925 + 0.0467x$.[11]

B. Data collection

Using Pd-filtered $AgK\alpha$ radiation, the full intensity profiles of the Bragg reflections were recorded in the continuous ω—2θ scan mode with an ω-scan speed of $0.01°\,s^{-1}$ on an automated four-circle diffractometer, at room temperature.

1. $TiC_{0.94}$

A complete sphere of reflections was measured out to a limit of 1.73 $Å^{-1}$ in $(\sin\theta)/\lambda$, using a scan width of $1.60° + 0.80°\tan\theta$ in ω, and a detector window of $1.00° \times 1.00°$ angular height and width.

The intensity of each low-order reflection, with $(\sin\theta)/\lambda \leq 0.47$ $Å^{-1}$, was recorded at 13 values of the azimuthal angle ψ around the scattering vector ($-90° \leq \psi \leq 90°$, $\Delta\psi = 15°$), wherever accessible from one mounting of the crystal. Exceptional care was taken in the instrument-crystal alignment to ensure that the diffracted beam always fell on the same area of the detector. This was checked by using photographic films placed at the position of the detector and comparing the size of a single spot of the reflection $\bar{2}0\bar{2}$ at $\psi = 0°$ with that of superimposed spots, produced when ψ is increased from 0° to 180° in 15° steps. The uniformity of response of the scintillation detector over its active area ($6 \times 1.5°$) was found to be constant within statistical errors.[12]

A correction for the overall dead time τ of the counting chain was applied as $n_t = n_o[1 - (\tau/t)n_o]$, where n_t is the number of counts per step in the reflection scan without counting loss, n_o is the observed number of counts, and t is the measurement time per step. τ was determined to be 0.18×10^{-5} s using a method, analogous to Ref. 13, in which all reflections with $(\sin\theta)/\lambda \leq 0.52$ $Å^{-1}$ were measured successively with and without a 0.030-mm-thick Pd attenuator foil in the diffracted beam. The ratio of the respective corrected intensities was plotted versus the difference in the corrected intensities, and the dead-time correction τ was adjusted to make a zero slope.

The stability of the instrument was monitored. The intensities of three standard reflections, 400, $\bar{1}\,3\,\bar{1}$, and $\bar{1}\,\bar{1}\,5$, measured at 100-min intervals showed a steady decrease and, at the end of the 16 days of measurement, were reduced by 3.7% (there being no significant difference between the three reflections), thus necessitating scaling of the data by linear interpolation. The smoothed scale factor for the drift in standards is calculated from the ratio of the sums of the three standard intensities, averaged over the actual plus the five previous and the five following values, to the sum of the three standard intensities at the beginning of the experiment.

No corrections were made for diffuse scattering due to crystal defects or atomic thermal motion. The influence of the latter effect on the measured Bragg intensities was estimated to be very small. In particular, a calculation with the program TDS2 (Ref. 14) using the elastic constants of TiC from a tabulated source[15] showed that the effect was less than 4% at the highest scattering angles in our experiment. Since the elastic anisotropy parameter for TiC has a value of 0.875, which is quite close to the isotropic value, the lack of a thermal diffuse scattering correction will make itself felt almost entirely in the spherically symmetrical parameters of an atomic model.

2. $TiN_{0.99}$

A complete sphere of reflections was measured out to a limit of 1.62 $Å^{-1}$ in $(\sin\theta)/\lambda$ using a scan width of $2.50° + 0.45°/\tan\theta$ in ω, and a detector window of $1.50° \times 3.00°$. The reflections with $(\sin\theta)/\lambda \leq 1.02$ $Å^{-1}$ were remeasured with the x-ray tube running at a quarter of the normal power (5 versus 20 mA, 60 kV) to keep the count rate below 30 000 s^{-1}. ψ scans were made under the same conditions with $-180° \leq \psi \leq 180°$, $\Delta\psi = 10°$, for all reflections 111, 200, 220, 311, 222, 400, 333, 440, and 600, and their symmetry-related equivalents, and with

$-90° \leq \psi \leq 90°$, $\Delta\psi = 15°$ for the remaining reflections with $(\sin\theta)/\lambda \leq 0.80$ Å^{-1}, apart from $\{533\}$.

The intensities of three standard reflections 600, $\bar{3}\bar{3}\bar{3}$, and $\bar{1}\bar{1}5$, measured at intervals of 100 min, varied over the whole data-collection time by at most 1.5% for the high-power setting and 2.3% for the low one. The data were scaled for these variations.

Suitable reflections from both the high- and low-power sets were used to estimate an overall dead-time correction of $\tau = 0.19 \times 10^{-5}$ s, applied to each single step of a reflection scan. As with the carbide crystal, no corrections were made for the supposedly minimal effects of diffuse scattering due either to crystal defects or atomic thermal motion.

C. Profile analysis and quality of the data

The scan profiles, divided into from 80 to 113 steps, were analyzed to give the integrated intensity I and its standard deviation $\sigma(I)$, using the minimum $\sigma(\text{count})/I$ algorithm.[16–18] For all reflections the ratios $I/\sigma(I)$ were larger than 22. The variance $\sigma^2(I) = \sigma^2(\text{count}) + [p \times (\text{total counts})]^2$ was calculated with a value of p determined from the intensity fluctuations in the standard reflections after scaling for the long-term variations and p was found to be 0.0020 for $TiC_{0.94}$ and 0.0025 for $TiN_{0.99}$.

The integrated intensities were corrected for Lorentz-polarization effects, and for absorption by a sphere with linear absorption coefficients μ of 4.643 mm^{-1} for $TiC_{0.94}$ and 4.960 mm^{-1} for $TiN_{0.99}$. Absorption-weighted mean path lengths $\bar{T}$ were computed[19] for subsequent use in extinction corrections.

Altogether, 3947 reflection profiles were processed for $TiC_{0.94}$, corresponding to 122 symmetry-independent reflections and 6335 for $TiN_{0.99}$, corresponding to 98 unique reflections. The internal consistency of both data sets was estimated by calculating the overall agreement indices,

$$R_{\text{int}} = \sum^{h,k,l} (I_r - \langle I \rangle_r) \Big/ \sum^{h,k,l} I_r \ ,$$

$$R_{w,\text{int}} = \left[\sum^{h,k,l} w(I_r - \langle I \rangle_r)^2 \Big/ \sum^{h,k,l} wI_r^2 \right]^{1/2} ,$$

where the $\langle I \rangle_r$ are the average intensities of symmetry-related equivalents, including reflections recorded at $\psi \neq 0°$ and $w = 1/\sigma^2(I_r)$. The values found, prior to anisotropic extinction correction, are

$$R_{\text{int}} = 0.030 \text{ and } R_{w,\text{int}} = 0.025 \text{ for } TiC_{0.94} \ ,$$

$$R_{\text{int}} = 0.021 \text{ and } R_{w,\text{int}} = 0.013 \text{ for } TiN_{0.99} \ .$$

The agreement between the mean intensities and the individual measurements was poorer among the low-order reflections than the high-order ones, indicative of the presence of anisotropic extinction as discussed in Sec. III B 3. The largest values were $R_{\text{int}}(111) = 0.104$ and $R_{\text{int}}(200) = 0.095$ for $TiC_{0.94}$, and $R_{\text{int}}(200) = 0.083$ and $R_{\text{int}}(220) = 0.060$ for $TiN_{0.99}$.

III. ANALYSIS OF THE DATA

A. Rudimentary model and preliminary results

The electron densities of $TiC_{0.94}$ and $TiN_{0.99}$ were first described by the conventional model of superposed spherical (free) neutral atoms, and a preliminary structure refinement[20] was performed by the full matrix least-squares technique on symmetry-averaged data. The parameters refined included one scale factor k for $TiC_{0.94}$ and two for $TiN_{0.99}$, isotropic (by symmetry) thermal parameters $\langle u^2 \rangle_{\text{Ti}}$ and $\langle u^2 \rangle_X$, X=C,N, a population parameter of the nonmetal site, $\not{\kappa}_X$, to account for nonstoichiometry, and a parameter g, to account for an isotropic extinction effect dominated by a Lorentzian mosaic-spread distribution.[21–24] Anomalous dispersion corrections for $AgK\alpha_1$ were applied. The function minimized by the least-squares normal-equation technique was

$$\sum_i w_i (|F_r|_i - |F_c|_i / k_i)^2 \ ,$$

F_r being the observed structure factors on an arbitrary scale, $w_i = 1/\sigma^2(F_r)_i$, the weights computed from the estimated variance for the observed symmetry-equivalent measurements, and $|F_0(hkl)|$ [$= k\,|F_r(hkl)|$] and $|F_c(hkl)|$, the observed and calculated structure factors, respectively, on an absolute scale, but affected by extinction and anomalous dispersion. The degree of fit between the model and the data was measured by the following indicators: the residual R,

$$R = \sum_{i=1}^{m} |\Delta|_i \Big/ \sum_{i=1}^{m} |F_o|_i \ ,$$

the weighted residual R_w,

$$R_w = \left[\sum_{i=1}^{m} \omega_i \Delta_i^2 \Big/ \sum_{i=1}^{m} \omega_i |F_o|_i^2 \right]^{1/2} ,$$

the goodness of fit, S, and the d statistic,[25]

$$S = \left[\sum_{i=1}^{m} \omega_i \Delta_i^2 / (m-n) \right]^{1/2} ,$$

$$d = \sum_{i=2}^{N} (\Delta_i - \Delta_{i-1})^2 \Big/ \sum_{i=1}^{N} \Delta_i^2 \ ,$$

where $\Delta_i = |F_o|_i - |F_c|_i$, $\omega_i = w_i/k_i^2$, m is the number of observations, and n is the number of parameters refined. The results of the refinements are summarized in Table I for $TiC_{0.94}$ and in Table II for $TiN_{0.99}$. For both compounds, R and R_w were below 1%, while the goodness-of-fit parameters were relatively high ($S > 4$, ideal value $S = 1$). This reflects a generally good agreement between the observed and calculated structure factors, except for the strong low-order reflections which have Δ's as large as -1.18 for $TiC_{0.94}$ and $+2.21$ for $TiN_{0.99}$.

As expected for crystals with such high Debye temperatures (for TiC, 940 K, from elastic constant measurements[15]), the atomic thermal vibration amplitudes are small, having $\langle u^2 \rangle$ values of approximately 0.003 Å^2. In $TiC_{0.94}$, the thermal parameter of the metal,

TABLE I. Atomic parameters and agreement factors for $TiC_{0.94}$. Estimated standard deviations are given in parentheses. Refinement marked "ext" includes anisotropic extinction correction according to the Flack and Dunand[36] model. Refinement marked "no ext" was subsequently performed on extinction-corrected and -averaged data.

$TiC_{0.940}$	Rudimentary model	Sophisticated model ext	Sophisticated model no ext
k	0.1270(1)	0.1252(7)	1.0002(23)
$\langle u^2\rangle_{Ti}$ (Å^2)	0.003 46(2)	0.002 39(3)	0.002 38(2)
x_D		0.022 46	0.022 46(43)
$\langle u^2\rangle_C$(Å^2)	0.003 19(9)	0.003 30(8)	0.003 35(8)
f_C	0.920(9)	0.9388	0.939(9)
Extinction	$g=0.404(17)$[a]	b	
p_{4s}		1.26(54)	0.44(40)
$p_{t_{2g}}$		0.65(11)	0.76(4)
p_{e_g}		0.73(11)	0.75(4)
κ_{4s}		0.92(16)	0.94(10)
$\kappa_{t_{2g}}$		1.89(24)	1.77(8)
κ_{e_g}		1.53(10)	1.47(7)
p_{2s}		2.46(50)	3.07(37)
p_{2p}		3.00(76)	3.11(63)
κ_{2s}		0.86(4)	0.79(5)
κ_{2p}		1.20(9)	1.23(7)
Q(Ti)		1.37(45)	2.05(38)
Q(C)		−1.46(37)	−2.18(41)
$p(3d)$ spherical		1.08(20)	1.27(6)
$p(3d)$ nonspherical		0.30(15)	0.24(5)
$p(3d)$ total		1.37(15)	1.51(5)
R	0.008	0.0087	0.0025
R_w	0.008	0.0101	0.0027
S	4.25	1.79	1.73
m	122	3823	122
n	5	31	12
d	1.55	1.23	0.99
R_{int}	0.030	0.015	
$R_{w,int}$	0.025	0.018	
m unique	122	122	

[a] 10^4 rad^{-1}.
[b] See Table III.

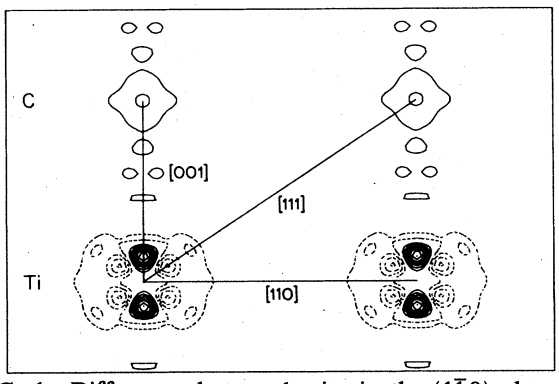

FIG. 1. Difference electron density in the $(1\bar{1}0)$ plane of $TiC_{0.94}$. Spherical atom, rudimentary model subtracted from the observed density ($0 \le s \le 1.728$ Å^{-1}). Contour intervals, $0.20e$ Å^{-3}. Positive contours, solid line; negative contours, dashed line; zero contours omitted.

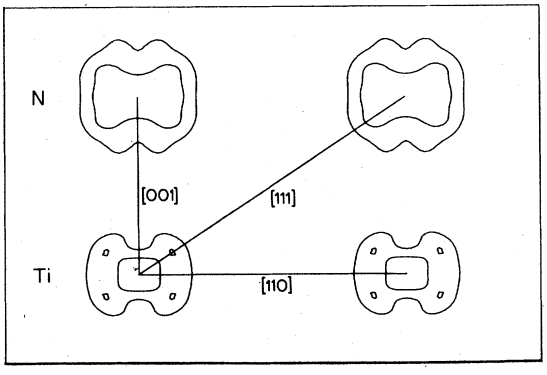

FIG. 2. Difference electron density in the $(1\bar{1}0)$ plane of $TiN_{0.99}$ ($0 \le s \le 1.612$ Å^{-1}). Otherwise, same specifications as in Fig. 1. Note that there are no significant negative contours in this section.

TABLE II. Atomic parameters and agreement factors for $TiN_{0.99}$ (for specifications, see Table I).

$TiN_{0.992}$	Rudimentary model	Sophisticated model ext	Sophisticated model no ext
k_1	0.064 19(8)	0.0638(1)	1.0082(18)
k_2		0.0642(1)	
$\langle u^2\rangle_{Ti}$ (Å^2)	0.003 01(1)	0.003 02(1)	0.002 94(1)
$\langle u^2\rangle_N$ (Å^2)	0.003 25(4)	0.003 17(4)	0.003 08(12)
f_N	1.001(4)	0.9928	0.990(19)
Extinction	$g=0.148(4)$[a]	b	
p_{4s}		1.88(64)	1.09(38)
$p_{t_{2g}}$		0.51(23)	0.65(5)
p_{e_g}		0.28(11)	0.35(4)
κ_{4s}		0.90(6)	0.91(6)
$\kappa_{t_{2g}}$		1.29(11)	1.40(8)
κ_{e_g}		1.24(13)	1.42(12)
p_{2s}		1.73(28)	1.81(65)
p_{2p}		4.60(57)	5.12(66)
κ_{2s}		0.89(2)	0.78(8)
κ_{2p}		0.95(2)	0.96(6)
Q(Ti)		1.33(53)	1.91(34)
Q(N)		−1.34(38)	−1.93(37)
$p(3d)$ spherical		0.70(29)	0.88(11)
$p(3d)$ nonspherical		0.09(25)	0.12(9)
$p(3d)$ total		0.79(20)	1.00(7)
R	0.005	0.0066	0.0023
R_w	0.004	0.0080	0.0022
S	4.40	1.79	2.95
m	98	6643	98
n	5	32	13
d	1.03	1.04	1.48
R_{int}	0.021	0.012	
$R_{w,int}$	0.013	0.011	
m unique	98	98	

[a] 10^4 rad^{-1}.
[b] See Table III.

$\langle u^2\rangle_{Ti}=0.003\,46$ Å^2, appears suspiciously large when compared to that of the nonmetal, $\langle u^2\rangle_C=0.003\,19$ Å^2, and to the parameters in $TiN_{0.99}$, $\langle u^2\rangle_{Ti}=0.003\,01$ Å^2 and $\langle u^2\rangle_N=0.003\,25$ Å^2. The refined site-occupancy factors are insignificantly different from those obtained from chemical analysis.

Conspicuous differences between the carbide and the nitride crystals become apparent on the difference electron density ($\Delta\rho$) maps, as defined by

$$\Delta\rho(x,y,z)=\frac{1}{V}\sum_{h,k,l}\Delta(hkl)\times\exp\{-2\pi i[hx+ky+lz+\alpha(hkl)]\}\ .$$

These represent, via a Fourier transform, the difference between the observed electron density and the model density. A section, $(1\,\bar{1}\,0)$, containing the three major directions of interest [001], [110], and [111], is represented in Fig. 1 for $TiC_{0.94}$ and in Fig. 2 for $TiN_{0.99}$. While in the nitride the electron density corresponds, to a good approximation, to that of superposed isolated neutral atoms, judging from the occurrence of only eight small humps of deformation density around the Ti atoms, having a maximum of $0.41e$ Å^{-3} at 0.44 Å along the ⟨111⟩ directions, in the carbide, on the other hand, large deformations occur around the metal atom in the form of six lobes of positive density having a maximum of $1.41e$ Å^{-3} at 0.30 Å along the ⟨100⟩ directions and of eight holes of negative density having a minimum of $-0.85e$ Å^{-3} at 0.32 Å along the ⟨111⟩ directions.

Thus the picture which emerges at this stage of the analysis suggests a redistribution of $3d$ electrons on the metal-atom sites (octahedral symmetry) into orbitals of e_g symmetry (i.e., charge density pointing towards the nearest C-atom sites) in the carbide, and, conversely, but to a lesser extent, into orbitals of t_{2g} symmetry (i.e., charge density pointing towards the tetrahedral holes in

the fcc Ti-atom network) in the nitride. By contrast, no significant charge asphericity is observed around the nonmetal-atom sites. Moreover, no other buildup of charge density can be found.

In order to produce a more realistic scattering model, the nonspherical effects detected above were analyzed in greater detail. As shown in Fig. 3 the deformation density maxima of $TiC_{0.94}$ contain a large contribution from high-order reflections. Their heights in the (100) section increase from $0.31e$ Å^{-3} to $0.94e$ Å^{-3} and their location is shifted from 0.43 to 0.29 Å from the Ti nucleus when the cutoff window moves from $0.7 \leq (\sin\theta)/\lambda \leq 1.10$ Å^{-1} to $1.30 \leq (\sin\theta)/\lambda \leq 1.70$ Å^{-1}. This behavior is at variance with the trend expected from bonding features associated with $3d$ orbitals and indicates that a fraction of the Ti atoms could be statistically displaced from their average positions along ⟨100⟩. As shown in the Appendix the anisotropy in the d shell and static (or dynamic) atomic displacements can be recognized and separated from one another owing to their different dependence on $(\sin\theta)/\lambda$. A rough estimate for $TiC_{0.94}$ indicates displacement amplitudes of about 0.1 Å. The displacements are most likely of static nature and due to vacancies on the nonmetal sites. Dynamic displacements due to anisotropic anharmonic thermal vibrations[26] are less likely in this compound because of its high Debye temperature and the absence of structural phase transformations. Consequently, a more sophisticated model of the compounds was constructed.

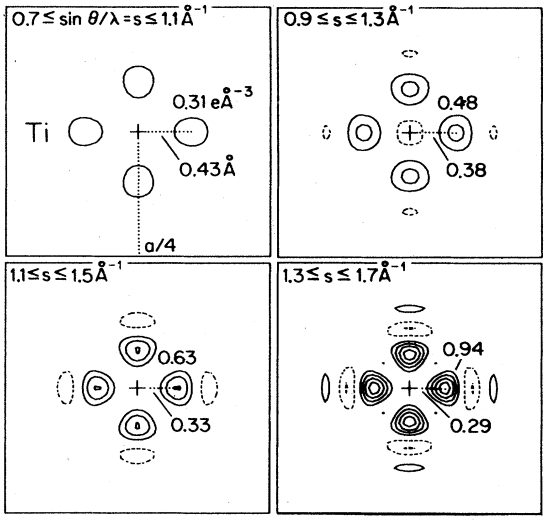

FIG. 3. Evolution of the residual electron density in $TiC_{0.94}$ as a function of the $(\sin\theta)/\lambda$ cutoff window. Contour intervals, $0.20e$ Å^{-3}. Positive contours, solid line; negative contours, dashed line; zero contours omitted.

B. Sophisticated model

This model allows for three effects not considered in Sec. III A. First, the electron density distribution of the individual atoms was broken down into a core and orbital contributions of the valence shell. For the metal, this may correspond to a nonspherical electron density distribution of a single atom. Second, a limited model of partial atomic static displacements around the mean metal-atom site was incorporated. Third, an anisotropic extinction correction was applied.

The expression used for the calculated structure factor F_c is

$$F_c(hkl)=\{4\not{e}_M f_M(hkl)\exp(-8\pi^2\langle u^2\rangle_M s^2)+8\not{e}_D f_D(hkl)\exp(-8\pi^2\langle u^2\rangle_D s^2)$$
$$\times[\cos(2\pi h x_D)+\cos(2\pi k x_D)+\cos(2\pi l x_D)]\pm 4\not{e}_X f_X(hkl)\exp(-8\pi^2\langle u^2\rangle_X s^2)\}y_{\rm calc}(hkl,\psi)\ .$$

The contribution of the nonmetal atom is positive when hkl are all even indices and negative when all are odd. M denotes the metal atom in (0,0,0) [site symmetry $m\,3m(O_h)$], D the displaced metal atoms in $(x_D,0,0)$ [site symmetry $4mm(C_{4v})$], and X the nonmetal atom in $(\frac{1}{2},\frac{1}{2},\frac{1}{2})$ (site symmetry $m\,3m$). $f(hkl)$ is the nonspherical atomic scattering factor, $\not{e}$ the site-occupancy parameter, $\langle u^2\rangle$ the isotropic temperature factor, $s=(\sin\theta)/\lambda$, and $y_{\rm calc}(hkl,\psi)$ is the anisotropic extinction correction.

1. Atomic scattering factor

Atomic nonsphericity and charge-transfer effects were modeled by refining the electronic core and valence populations p of the 18-electron Ar core, the $4s$, $3d$ e_g, and t_{2g} orbitals of the metal atoms, the two-electron He core, and the $2s$ and $2p$ orbitals of the nonmetal atoms. The formalism for the scattering by s, p, and d electrons is that of McWeeny,[27] Freeman,[28] Weiss and Freeman,[29] and Dawson.[30,31] The relevant core and single-electron $\langle j_0\rangle_{s,p,d}$, $\langle j_2\rangle_d$, and $\langle j_4\rangle_d$ scattering curves were taken from tabulated sources.[9,32] Because such theoretical scattering curves apply to isolated atoms, for atoms in a crystal environment it is necessary to allow for some refinement of the scattering-curve shape. To this end, radial expansion-contraction coefficients κ (Ref. 33) are applied which specify that the "real" scattering factor at $(\sin\theta)/\lambda=s$ is the free-atom scattering factor at $(\sin\theta)/\lambda=s/\kappa$. Hence, the valence populations and the expansion-contraction parameters that are obtained will refer to the atomic scattering curves that are used. The expressions for the scattering factors, including anomalous dispersion, are

$$f_M(hkl)=p_{\rm Ar}f_{\rm Ar}^{\rm core}(s/\kappa_{\rm Ar})+p_{4s}\langle j_0(s/\kappa_{4s})\rangle_{4s}+p_{t_{2g}}\langle j_0(s/\kappa_{t_{2g}})\rangle_{3d}+p_{e_g}\langle j_0(s/\kappa_{e_g})\rangle_{3d}$$
$$+\tfrac{3}{2}A(\beta,\gamma)[p_{e_g}\langle j_4(s/\kappa_{e_g})\rangle_{3d}-p_{t_{2g}}\langle j_4(s/\kappa_{t_{2g}})\rangle_{3d}]+f'_M+if''_M\ ,$$

where

$$A(\beta,\gamma)=\frac{h^4+k^4+l^4-3(h^2k^2+h^2l^2+k^2l^2)}{(h^2+k^2+l^2)^2},$$

$$f_X(hkl)=p_{\mathrm{He}}f^{\mathrm{core}}_{\mathrm{He}}(s/\kappa_{\mathrm{He}})+p_{2s}\langle j_0(s/\kappa_{2s})\rangle_{2s}+p_{2p}\langle j_0(s/\kappa_{2p})\rangle_{2p}+f'_X+if''_X .$$

Charge neutrality is imposed by the following constraint:

$$p_{t_{2g}}=Z_M-18p_{\mathrm{Ar}}-p_{4s}-p_{e_g}+f_X(Z_X-2p_{\mathrm{He}}-p_{2s}-p_{2p})/(f_M+6f_D) .$$

2. Static displacements of metal atoms

The probability of producing, at random, a configuration $MX_n\square_{6-n}$ from a sample of composition MX_x (M denotes metal, X denotes nonmetal),

$$MX_6{:}MX_5\square_1{:}MX_4\square_2{:}\cdots = x^6{:}6x^5(1-x){:}15x^4(1-x)^2{:}\cdots ,$$

where $\square$ represents a vacancy on the nonmetal site. For example, in $TiC_{0.94}$ there would be 69.0% TiC_6-, 26.4% $TiC_5\square_1$-, and 4.2% $TiC_4\square_2$-type configurations. However, studies on other more-carbon-deficient crystals have shown that the vacancies tend to separate,[34] so that one would expect less $TiC_n\square_{6-n}$ configurations with $n\leq 4$ than for the random distribution. This also implies less of the TiC_6 and more of the $TiC_5\square_1$ configurations. In our model, $MX_n\square_{6-n}$ configurations with $n\leq 4$ have been neglected by assuming that the crystal is built up exclusively of f_MMX_6 and $(1-f_M)MX_5\square_1$ octahedra. Hence, the static displacements along $\langle 100\rangle$ found in $TiC_{0.94}$ (see Appendix) illustrate a symmetrical relaxation of the first-neighbor metal atoms around each nonmetal vacancy. Consequently, the site-occupancy parameters may be constrained as follows:

$$f_D=1-f_X \quad \text{and} \quad f_M=1-6f_D .$$

Two other constraints have been applied to keep the problem tractable,

$$f_D(hkl)=f_M(hkl) \quad \text{and} \quad \langle u^2\rangle_D=\langle u^2\rangle_M .$$

Thus, additional electron redistribution or harmonic anisotropic thermal motion around displaced metal atoms have not been considered in this model.

3. Anisotropic extinction

Effects due to anisotropic extinction were apparent in the data sets of both crystals and showed up in both large but smooth variations of $|F_0|$ with an azimuthal rotation Ψ around the scattering vector that describe more or less pronounced figures of eight, and in considerable differences of $|F_o|$ among symmetry-equivalent reflections. The latter include discernible anisotropic differences between reflection-antireflection pairs (i.e., measured in the same diffraction plane as a function of ψ). The cumulative effect produces relative variations of up to $\pm 10\%$ in $TiC_{0.94}$ and $\pm 8\%$ in $TiN_{0.99}$ for the most intense ({200}) set of reflections, while the latter effect alone is responsible for differences of up to 4% and 5%, respectively.

An illustrative example is presented in Fig. 4 which shows the variation of the "observed" extinction factor $y_{\mathrm{obs}}=|F_0|/|F_{c,\mathrm{kin}}|$ ($F_{c,\mathrm{kin}}$ is the calculated kinematic structure factor) of the 200 and $\bar{2}00$ reflections of $TiC_{0.94}$ as a function of ψ. Note that the observed variations of $|F_o|$ among symmetry equivalents cannot be due to a breakdown of crystal symmetry, as the discrepancies vanish with increasing $(\sin\theta)/\lambda$ value and no measurable departure from $m3m$ symmetry was observed among high-order reflections.

In order to obtain satisfactory estimates of the structure factors, especially of the low-order reflections, and to reproduce the ψ-angle dependences, we found it necessary to resort to a very general model for the correction of anisotropic extinction effects. This model takes into account the anisotropies due both to the mosaic spread and the domain size, and treats both primary and secondary extinction. The anisotropic mosaic misorientations, represented by a symmetric rank-2 tensor Z' is described with the Thornley-Nelmes[35] form for the Lorentzian angular spread. Another symmetric rank-2 tensor (R') represents the ellipsoidal domain size, and two models were considered for the treatment of this type of secondary extinction. The commonly used model of Becker and Coppens,[21–23] which enters the calculations as $(\vec{u}\,^T\underline{R}\,\vec{u})^{-1/2}$, where $\vec{u}$ is a vector along the diffracted beam, and an alternative model that describes the broadening of the incident and diffracted beams using concepts familiar to powder diffraction as suggested by Flack and Dunand,[36] which uses a quadratic form $(\vec{v}\,^T\underline{R}^{-1}\vec{v})^{1/2}$, where $\vec{v}$ is a vector perpendicular to the incident beam in the plane of diffraction, gave similar re-

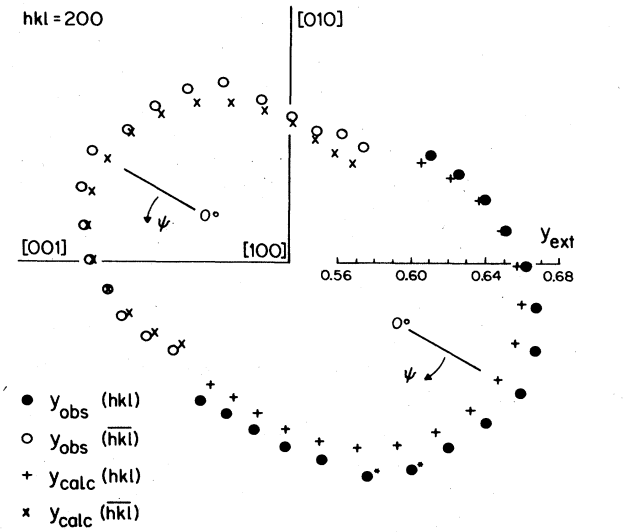

FIG. 4. Variations of y_{ext} as a function of the azimuthal angle ψ in $TiC_{0.94}$. For each measurement, a vector proportional in length to y_{ext} and parallel to the reflected ray direction has been projected onto the reflecting plane. Notice that the effect is exaggerated by focusing on the significant part of the variations (* denotes rejected from the refinement since $w\Delta^2\geq 36$).

sults, and so only those of the latter will be reported here. The treatment of primary extinction follows that of Becker and Coppens,[21–23] but with a path length of the incident and reflected beams as derived by Zachariasen.[24]

The anisotropic differences observed between Friedel pairs are not accounted for by current theories of anisotropic extinction. They must be due to inhomogeneity in the sample. It has been possible to model these differences by using modified tensors $\underline{Z}'=\underline{Z}(1+\vec{h}\cdot\vec{v}\,\vec{z}/|\vec{h}|)$ and $\underline{R}'=\underline{R}(1+\vec{h}\cdot\vec{v}\,\vec{r}/|\vec{h}|)$, where $\vec{h}$ is a reciprocal-lattice vector and $\vec{v}\,\vec{z}$ and $\vec{v}\,\vec{r}$ are refineable parameters, thus assuming a monodirectional gradient in both the domain size and mosaic angular spread across the crystals. More details are given elsewhere.[36]

Finally, differences in extinction effects between the surface and the interior of the crystals were taken into account, following Le Page and Gabe,[37] by assuming that the surface layer does not suffer from extinction, due to grinding, and refining that volume fraction x of the crystal. Extinction corrections assuming an homogeneous mosaicity over the total crystal volume were found to result in an overcorrection of the most extinct reflections and an undercorrection of the less extinct ones.

4. *Structure refinement*

A set of programs[38] was written by one of us (H.D.F.) for the refinement of the above-mentioned variables. The function

$$\sum_i w_i(|F_r|_i-|F_c|_i/k_i)^2 ,$$

with $w_i=1/\sigma^2(F_r)_i$, was minimized by using a quasi-Newton routine from the Numerical Algorithms Group (NAG) library[39] in which derivatives are calculated by finite differences. The atomic parameters obtained in the conventional refinement were used as starting values together with those values of isotropic extinction which correspond to a minimum in the observed S-shaped valley of the minimized function versus $\underline{Z}$ and $\underline{R}^{-1}$. These starting values were found to be critical for a successful minimization. The first part of the refinement was based on the complete data sets. Weights proportional to the reciprocal of the variance $\sigma^2(F_r)$ computed from the variance $\sigma^2(I)$ (cf. Sec. II C) have been used. Near convergence, a few iterations of refinement were run with k, x_D, and $\not{\kappa}_X$ as the sole variables, using only reflections with $(\sin\theta)/\lambda\geq 1.20$ Å^{-1}, where the contribution of the valence electrons becomes negligible. Both x_D and $\not{\kappa}_X$ were kept constant for the remainder of the refinement with the restriction that as no significant static displacements were detected in $TiN_{0.99}$, the parameter x_D was set to zero. In the very last iterations we found it convenient to exclude all those reflections which had large weighted differences, $\omega\Delta^2\geq 36$, in order to accelerate convergence. From inspection of the relevant azimuthal scan data, it became apparent that part of the rejected, low-order reflections was affected by multiple reflection. Altogether, about 3.0% of the data of $TiC_{0.94}$ and 1.5% of those of $TiN_{0.99}$ with $36\leq\omega\Delta^2\leq 440$ were rejected. Convergence was considered complete when the variation of the minimized function was less than 10 parts per million over five consecutive iterations.

The results of this refinement are summarized in Table I for $TiC_{0.94}$, in Table II for $TiN_{0.99}$ for the atomic parameters under the headings "ext," and in Table III for the extinction parameters of both $TiC_{0.94}$ and $TiN_{0.99}$. The estimated standard deviations of the parameters have been computed from an inversion of the matrix of the second derivatives.

The second part of the refinement was based on one unique set of averaged data, corrected for anisotropic extinction and put on a tentative absolute scale (i.e., kF_r/y_{calc}) and assigned weights derived from the estimated variance for the observed symmetry equivalents. For $TiC_{0.94}$, x_D and $\not{\kappa}_C$ were kept constant, while for $TiN_{0.99}$, $\not{\kappa}_N$ was allowed to vary. The results are given in Tables I and II under the headings "no ext." A number of pairs of parameters suffered from large correlations, namely, in $TiC_{0.94}$, k and U_{Ti}, −0.97; p_{2p} and U_C, −0.89; κ_{2s} and p_{2p}, −0.91; κ_{2p} and p_{2p}, −0.98; in TiN, k and U_{Ti}, −0.95; κ_{2s} and $\not{\kappa}_N$, 0.92; κ_{2p} and p_{2s}, 0.96; κ_{2p} and $\not{\kappa}_N$, −0.89. A list of the final observed and calculated kinematic structure factors is given in Tables IV and V.

IV. RESULTS AND DISCUSSION

Several indicators for the degree of fit to the data have been employed to check the quality of the various refinements. Care must be exercised when comparing them since the number of parameters varied, and the number of observations, their actual magnitudes, and their weights might change from model to model.

The corrections for the effects of anisotropic extinction

TABLE III. Anisotropic extinction parameters for $TiC_{0.94}$ and $TiN_{0.99}$. Z' is in units of 10^{-8} rad^2; $(R')^{-1}$ is in units of μm^2.

	TiC ext	TiN ext
Z'_{11}	8.8(9)	185.(24)
Z'_{22}	18.9(20)	35.(4)
Z'_{33}	13.0(13)	36.(4)
Z'_{12}	9.6(11)	10.(2)
Z'_{13}	−6.3(7)	−37.(5)
Z'_{23}	−4.7(6)	5.(1)
vz_1	0.01(3)	−0.04(2)
vz_2	0.18(2)	−0.58(2)
vz_3	0.44(2)	−0.03(3)
$(R'-1)_{11}$	41.3(16)	6.7(6)
$(R'-1)_{22}$	18.7(12)	4.9(4)
$(R'-1)_{33}$	15.7(11)	5.3(4)
$(R'-1)_{12}$	−7.6(3)	−1.6(2)
$(R'-1)_{13}$	3.3(3)	1.7(2)
$(R'-1)_{23}$	−2.1(2)	−3.3(2)
vr_1	0.12(2)	0.04(2)
vr_2	−0.15(2)	0.52(3)
vr_3	−0.16(2)	0.11(3)
x	0.020(5)	0.13(2)

TABLE IV. Observed and calculated kinematic structure factors for $TiC_{0.94}$.

h	k	l	s	F_o	F_c	$\sigma(F_o)$	Δ
1	1	1	0.200	47.71	48.02	0.07	−0.31
2	0	0	0.231	74.19	74.61	0.12	−0.42
2	2	0	0.327	59.27	59.18	0.06	0.09
3	1	1	0.383	36.34	36.23	0.02	0.11
2	2	2	0.400	50.15	50.12	0.07	0.04
4	0	0	0.462	44.55	44.41	0.04	0.13
3	3	1	0.503	28.49	28.43	0.03	0.05
4	2	0	0.516	40.22	40.12	0.06	0.10
4	2	2	0.566	36.95	36.91	0.06	0.04
5	1	1	0.600	24.09	24.16	0.02	−0.07
3	3	3	0.600	23.93	23.94	0.02	−0.02
4	4	0	0.653	32.51	32.46	0.06	0.05
5	3	1	0.683	21.18	21.23	0.02	−0.06
4	4	2	0.693	30.58	30.74	0.05	−0.16
6	0	0	0.693	30.86	30.97	0.08	−0.12
6	2	0	0.730	29.42	29.44	0.03	−0.02
5	3	3	0.757	19.20	19.19	0.02	0.01
6	2	2	0.766	28.04	28.08	0.03	−0.04
4	4	4	0.800	26.74	26.77	0.06	−0.03
5	5	1	0.825	17.58	17.65	0.02	−0.07
7	1	1	0.825	17.79	17.82	0.02	−0.03
6	4	0	0.833	25.69	25.77	0.03	−0.09
6	4	2	0.864	24.69	24.73	0.02	−0.04
5	5	3	0.887	16.29	16.30	0.02	−0.01
7	3	1	0.887	16.43	16.42	0.02	0.01
8	0	0	0.924	23.05	23.08	0.04	−0.02
7	3	3	0.945	15.22	15.21	0.02	0.01
6	4	4	0.952	21.98	22.00	0.03	−0.02
8	2	0	0.952	22.16	22.19	0.02	−0.03
6	6	0	0.980	21.13	21.23	0.05	−0.10
8	2	2	0.980	21.34	21.34	0.02	−0.01
7	5	1	1.000	14.14	14.16	0.02	−0.01
5	5	5	1.000	14.03	14.08	0.03	−0.05
6	6	2	1.007	20.43	20.44	0.03	−0.01
8	4	0	1.033	19.76	19.79	0.02	−0.03
9	1	1	1.052	13.37	13.36	0.02	0.01
7	5	3	1.052	13.19	13.17	0.02	0.02
8	4	2	1.058	19.05	19.06	0.02	−0.01
6	6	4	1.083	18.26	18.28	0.03	−0.03
9	3	1	1.102	12.44	12.41	0.02	0.03
8	4	4	1.131	17.11	17.06	0.03	0.06
9	3	3	1.149	11.62	11.55	0.03	0.07
7	5	5	1.149	11.49	11.43	0.03	0.06
7	7	1	1.149	11.47	11.47	0.03	−0.01
10	0	0	1.155	16.64	16.65	0.05	−0.02
8	6	0	1.155	16.52	16.47	0.02	0.05
8	6	2	1.178	15.89	15.88	0.02	0.01
10	2	0	1.178	16.05	16.05	0.03	0.00
7	7	3	1.195	10.72	10.68	0.03	0.04
9	5	1	1.195	10.80	10.76	0.02	0.03
10	2	2	1.200	15.48	15.47	0.03	0.02
6	6	6	1.200	15.24	15.26	0.05	−0.01
9	5	3	1.238	10.11	10.02	0.02	0.08
8	6	4	1.244	14.25	14.24	0.02	0.00
10	4	0	1.244	14.42	14.39	0.03	0.04
10	4	2	1.265	13.92	13.87	0.02	0.04
11	1	1	1.281	9.56	9.54	0.03	0.01
7	7	5	1.281	9.31	9.28	0.02	0.02
8	8	0	1.307	12.82	12.86	0.04	−0.03
9	7	1	1.322	8.76	8.75	0.02	0.01
9	5	5	1.322	8.73	8.72	0.03	0.01

TABLE IV. (*Continued*).

h	k	l	s	F_o	F_c	$\sigma(F_o)$	Δ
11	3	1	1.322	8.97	8.89	0.02	0.08
8	8	2	1.327	12.43	12.41	0.03	0.03
10	4	4	1.327	12.48	12.46	0.03	0.01
10	6	0	1.347	12.09	12.05	0.02	0.04
8	6	6	1.347	12.00	11.94	0.03	0.06
9	7	3	1.362	8.16	8.16	0.02	0.00
11	3	3	1.362	8.29	8.29	0.03	−0.01
10	6	2	1.366	11.71	11.63	0.02	0.07
8	8	4	1.386	11.21	11.17	0.02	0.05
12	0	0	1.386	11.52	11.44	0.04	0.08
7	7	7	1.400	7.54	7.57	0.06	−0.03
11	5	1	1.400	7.73	7.74	0.02	−0.01
12	2	0	1.405	11.04	11.04	0.02	0.00
10	6	4	1.424	10.46	10.48	0.02	−0.02
12	2	2	1.424	10.71	10.66	0.03	0.04
9	7	5	1.438	7.11	7.12	0.02	0.00
11	5	3	1.438	7.22	7.23	0.02	−0.01
12	4	0	1.461	10.01	9.96	0.02	0.05
9	9	1	1.474	6.71	6.72	0.02	−0.01
12	4	2	1.479	9.62	9.62	0.02	0.00
10	8	0	1.479	9.52	9.50	0.02	0.02
8	8	6	1.479	9.47	9.41	0.02	0.06
10	8	2	1.497	9.18	9.18	0.02	0.00
11	5	5	1.510	6.31	6.32	0.02	−0.02
13	1	1	1.510	6.57	6.53	0.02	0.03
9	9	3	1.510	6.28	6.28	0.02	0.00
11	7	1	1.510	6.35	6.34	0.01	0.01
10	6	6	1.515	8.83	8.85	0.02	−0.02
12	4	4	1.532	8.67	8.70	0.02	−0.02
13	3	1	1.545	6.09	6.11	0.02	−0.02
9	7	7	1.545	5.81	5.84	0.02	−0.04
11	7	3	1.545	5.92	5.94	0.02	−0.02
12	6	0	1.549	8.42	8.43	0.02	−0.01
10	8	4	1.549	8.32	8.31	0.02	0.02
12	6	2	1.566	8.16	8.15	0.01	0.01
9	9	5	1.579	5.51	5.51	0.02	0.00
13	3	3	1.579	5.73	5.73	0.02	0.01
8	8	8	1.600	7.49	7.49	0.05	0.00
13	5	1	1.613	5.39	5.37	0.02	0.01
11	7	5	1.613	5.24	5.22	0.02	0.02
12	6	4	1.617	7.35	7.39	0.02	−0.04
14	0	0	1.617	7.54	7.60	0.02	−0.06
10	10	0	1.633	7.06	7.13	0.04	−0.07
10	8	6	1.633	7.08	7.06	0.02	0.02
14	2	0	1.633	7.35	7.36	0.03	−0.01
13	5	3	1.645	5.00	5.04	0.02	−0.05
11	9	1	1.645	4.91	4.94	0.02	−0.04
14	2	2	1.649	7.08	7.13	0.03	−0.05
10	10	2	1.649	6.88	6.90	0.02	−0.02
12	8	0	1.666	6.73	6.74	0.02	−0.01
9	9	7	1.677	4.54	4.57	0.02	−0.03
11	9	3	1.677	4.62	4.64	0.02	−0.02
12	8	2	1.681	6.53	6.53	0.01	0.00
14	4	0	1.681	6.65	6.69	0.03	−0.04
14	4	2	1.697	6.45	6.48	0.02	−0.03
10	10	4	1.697	6.21	6.27	0.03	−0.06
12	6	6	1.697	6.29	6.30	0.02	−0.02
13	7	1	1.709	4.44	4.47	0.02	−0.02
13	5	5	1.709	4.43	4.45	0.03	−0.02
11	7	7	1.709	4.31	4.34	0.03	−0.03
12	8	4	1.728	5.94	5.94	0.01	0.00

TABLE V. Observed and calculated kinematic structure factors for $TiN_{0.99}$.

h	k	l	s	F_o	F_c	$\sigma(F_o)$	Δ
1	1	1	0.204	42.23	42.42	0.03	−0.18
2	0	0	0.236	74.92	75.53	0.09	−0.61
2	2	0	0.333	59.53	59.41	0.03	0.12
3	1	1	0.391	33.45	33.36	0.01	0.08
2	2	2	0.408	50.26	50.13	0.03	0.14
4	0	0	0.472	44.18	44.10	0.04	0.08
3	3	1	0.514	26.80	26.84	0.01	−0.04
4	2	0	0.527	40.06	40.00	0.02	0.06
4	2	2	0.578	37.02	36.99	0.02	0.03
5	1	1	0.613	22.89	22.94	0.01	−0.05
3	3	3	0.613	22.94	22.99	0.01	−0.05
4	4	0	0.667	32.74	32.78	0.01	−0.04
5	3	1	0.697	20.48	20.47	0.01	0.00
4	4	2	0.707	31.21	31.21	0.02	0.00
6	0	0	0.707	31.03	31.15	0.02	−0.13
6	2	0	0.746	29.72	29.80	0.01	−0.08
5	3	3	0.773	18.67	18.69	0.01	−0.02
6	2	2	0.782	28.56	28.60	0.01	−0.04
4	4	4	0.817	27.49	27.52	0.04	−0.03
7	1	1	0.842	17.18	17.20	0.02	−0.02
5	5	1	0.842	17.23	17.23	0.02	−0.01
6	4	0	0.850	26.37	26.47	0.03	−0.10
6	4	2	0.882	25.48	25.51	0.02	−0.03
5	5	3	0.906	16.03	16.00	0.01	0.03
7	3	1	0.906	15.99	15.97	0.01	0.02
8	0	0	0.943	23.65	23.71	0.05	−0.05
7	3	3	0.965	14.89	14.88	0.02	0.01
8	2	0	0.972	22.86	22.90	0.02	−0.04
6	4	4	0.972	22.96	22.93	0.02	0.03
8	2	2	1.000	22.13	22.12	0.01	0.01
6	6	0	1.000	22.13	22.14	0.02	−0.01
5	5	5	1.021	13.82	13.89	0.02	−0.06
7	5	1	1.021	13.87	13.87	0.01	0.00
6	6	2	1.028	21.44	21.39	0.03	0.05
8	4	0	1.054	20.67	20.65	0.01	0.02
7	5	3	1.074	12.94	12.95	0.01	−0.01
9	1	1	1.074	12.98	12.92	0.03	0.07
8	4	2	1.080	19.99	19.95	0.01	0.03
6	6	4	1.106	19.37	19.29	0.02	0.08
9	3	1	1.125	12.11	12.06	0.01	0.05
8	4	4	1.155	18.07	18.01	0.02	0.06
9	3	3	1.173	11.29	11.27	0.02	0.02
7	7	1	1.173	11.34	11.28	0.02	0.06
7	5	5	1.173	11.31	11.28	0.02	0.02
8	6	0	1.179	17.41	17.41	0.01	0.00
10	0	0	1.179	17.37	17.39	0.03	−0.01
8	6	2	1.202	16.88	16.83	0.01	0.05
10	2	0	1.202	16.82	16.81	0.02	0.00
9	5	1	1.219	10.57	10.53	0.01	0.05
7	7	3	1.219	10.57	10.54	0.02	0.03
6	6	6	1.225	16.30	16.28	0.04	0.02
10	2	2	1.225	16.32	16.26	0.02	0.06
9	5	3	1.264	9.85	9.84	0.01	0.02
10	4	0	1.270	15.26	15.21	0.02	0.06
8	6	4	1.270	15.25	15.22	0.01	0.03
10	4	2	1.291	14.75	14.71	0.01	0.04
11	1	1	1.307	9.23	9.18	0.02	0.05
7	7	5	1.307	9.21	9.20	0.02	0.00
8	8	0	1.334	13.78	13.78	0.03	0.01
9	5	5	1.349	8.61	8.60	0.02	0.01
11	3	1	1.349	8.60	8.59	0.01	0.01

TABLE V. (*Continued*).

h	k	l	s	F_o	F_c	$\sigma(F_o)$	Δ
9	7	1	1.349	8.62	8.60	0.01	0.01
8	8	2	1.354	13.36	13.33	0.01	0.02
10	4	4	1.354	13.34	13.33	0.02	0.02
10	6	0	1.375	12.93	12.90	0.02	0.03
8	6	6	1.375	12.89	12.91	0.02	−0.01
9	7	3	1.390	8.06	8.05	0.01	0.01
11	3	3	1.390	8.05	8.04	0.02	0.00
10	6	2	1.395	12.51	12.49	0.01	0.02
8	8	4	1.415	12.15	12.09	0.01	0.05
12	0	0	1.415	12.09	12.08	0.04	0.02
7	7	7	1.429	7.54	7.55	0.02	−0.01
11	5	1	1.429	7.56	7.54	0.01	0.02
12	2	0	1.434	11.72	11.69	0.01	0.03
12	2	2	1.453	11.35	11.33	0.01	0.02
10	6	4	1.453	11.36	11.34	0.01	0.02
11	5	3	1.468	7.07	7.07	0.01	0.00
9	7	5	1.468	7.07	7.07	0.01	−0.01
12	4	0	1.491	10.65	10.64	0.02	0.01
9	9	1	1.505	6.65	6.64	0.01	0.02
10	8	0	1.510	10.30	10.32	0.01	−0.01
8	8	6	1.510	10.32	10.32	0.01	0.00
12	4	2	1.510	10.29	10.31	0.01	−0.02
10	8	2	1.528	9.96	10.00	0.01	−0.04
9	9	3	1.542	6.22	6.24	0.01	−0.01
13	1	1	1.542	6.22	6.22	0.01	−0.01
11	5	5	1.542	6.21	6.23	0.02	−0.03
11	7	1	1.542	6.23	6.23	0.01	0.00
10	6	6	1.546	9.66	9.70	0.01	−0.03
12	4	4	1.564	9.40	9.40	0.01	0.00
13	3	1	1.577	5.82	5.86	0.01	−0.04
11	7	3	1.577	5.81	5.87	0.01	−0.05
9	7	7	1.577	5.84	5.87	0.01	−0.02
12	6	0	1.582	9.10	9.12	0.01	−0.02
10	8	4	1.582	9.08	9.12	0.01	−0.04
12	6	2	1.599	8.75	8.85	0.01	−0.10
9	9	5	1.612	5.47	5.53	0.02	−0.06
13	3	3	1.612	5.45	5.52	0.02	−0.07

and of crystal inhomogeneity proved adequate, as can be seen from the much improved internal consistency of the data, $R_{\text{int}}=0.015$ after correction versus 0.030 before correction for $TiC_{0.94}$, and 0.012 versus 0.021 for $TiN_{0.99}$. Confirmation that the azimuthal angle dependencies of the low-order diffraction data and that the differences in magnitude between reflections and antireflections are satisfactorily reproduced can be found in the acceptable agreement between equivalents, e.g., $R_{\text{int}}(111)=0.021$ and $R_{\text{int}}(200)=0.026$ for $TiC_{0.94}$, and $R_{\text{int}}(200)=0.024$ and $R_{\text{int}}(220)=0.019$ for $TiN_{0.99}$ (cf. Sec. II C). A graphic representation is given in Fig. 4 for the 200 and $\bar{2}00$ reflections of $TiC_{0.94}$.

The low R values obtained attest to the correctness of the sophisticated model chosen, $R=0.0025$ for $TiC_{0.94}$ and 0.0023 for $TiN_{0.99}$, while the significant goodness-of-fit indices and Durbin-Watson d statistics underline a small but systematic oscillation of Δ versus $(\sin\theta)/\lambda$. $|\Delta|/|F_0|$ is always less than 1.0% or 1.2%, respectively. The relative smallness of these residuals does not warrant an extension of the model. The small values of the

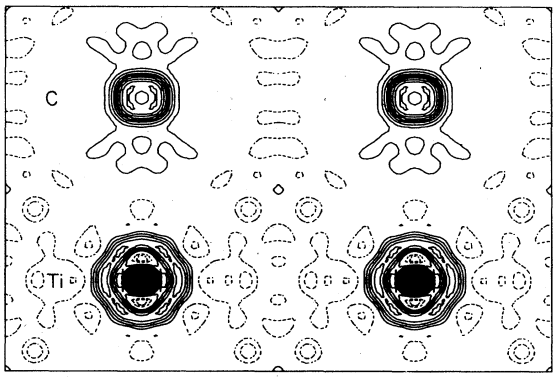

FIG. 5. Residual electron density in the $(1\bar{1}0)$ plane of $TiC_{0.94}$. Sophisticated model after the refinement "ext" subtracted from the observed density ($0\leq s\leq 1.728$ Å^{-1}). Contour intervals, 0.05e Å^{-3}. Positive contours, solid line; negative contours, dashed line; zero contours omitted.

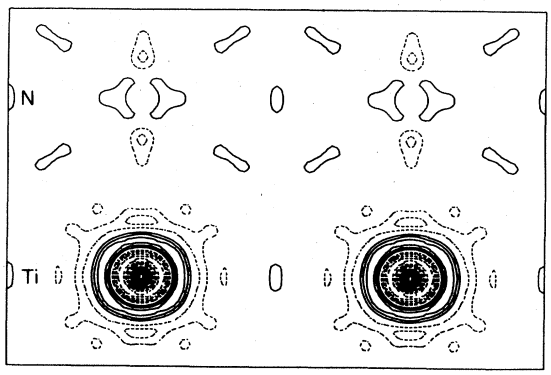

FIG. 6. Residual electron density in the $(1\bar{1}0)$ plane of $TiN_{0.99}$ ($0 \leq s \leq 1.612$ Å^{-1}). Otherwise, same specifications as in Fig. 5.

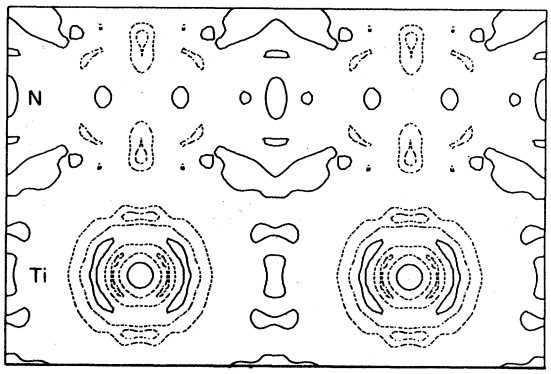

FIG. 8. Residual electron density in the $(1\bar{1}0)$ plane of $TiN_{0.99}$. Same specifications as in Fig. 7, with $0 \leq s \leq 1.612$ Å^{-1}.

Durbin-Watson d statistic, 0.99 and 1.48, for an ideal value of 2.00, means that the calculated standard deviations on some parameters may be somewhat underestimated.

A. Residual maps

The residual electron density maps computed after the "ext" refinement from the extinction-corrected and -averaged data still show substantial ripples of nearly spherical symmetry around the atomic sites, respectively, in Figs. 5 and 6 for $TiC_{0.94}$ and $TiN_{0.99}$, that supposedly reflect a slight bias in the refinement brought upon by including such a large number of low-order reflections (ψ scans). Since these low-order reflections have a poorer internal agreement than the higher-order ones [i.e., $\sigma(F)$'s in Tables IV and V], they are relatively downweighted in the subsequent refinement versus the unique data sets. This produces small changes in the atomic parameters (Tables I and II) and an improvement in the residual electron density (Figs. 7 and 8). The maximum and minimum values of the latter are $0.11e$ Å^{-3} and $-0.16e$ Å^{-3} in $TiC_{0.94}$, and 0.10 and $-0.12e$ Å^{-3} in $TiN_{0.99}$.

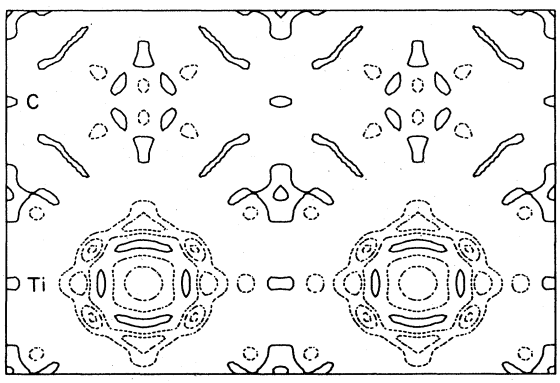

FIG. 7. Residual electron density in the $(1\bar{1}0)$ plane of $TiC_{0.94}$. Sophisticated model after the refinement "no ext" subtracted from the observed density. Contours as in Fig. 5.

B. Stoichiometry

The refined occupancy factors of the nonmetal sites $\nu_C = 0.939(9)$ and $\nu_N = 0.99(2)$ are in excellent agreement with their respective chemical analysis, $TiC_{0.940(5)}$ and $TiN_{0.992(5)}$.

C. Thermal vibration parameters

The mean-square amplitudes of thermal vibrations obtained from the sophisticated model are consistent with the respective atomic masses, $\langle u^2 \rangle_{Ti} = 0.002\,38(2)$ Å^2 versus $\langle u^2 \rangle_C = 0.003\,35(8)$ Å^2, and $\langle u^2 \rangle_{Ti} = 0.002\,94(1)$ Å^2 versus $\langle u^2 \rangle_N = 0.003\,08(12)$ Å^2, and compare well with the amplitudes from models describing experimental phonon-dispersion relations.[40] In the rudimentary model, the relaxation of the metal atoms around vacancies contribute to an apparent increase of about 45% of the temperature factor to $\langle u^2 \rangle_{Ti} = 0.003\,46(2)$ Å^2.

D. Static displacements of Ti atoms

The results of the sophisticated model imply that a fraction as large as 36% of the metal atoms in $TiC_{0.94}$ are displaced from their sublattice sites by 0.097(2) Å along [100]. By contrast, no evidence for displaced metal atoms was found in the more stoichiometric $TiN_{0.99}$, although 6% of the metal atoms are surrounded by a N-site vacancy. To the authors' knowledge there exists no report of significant concentrations of metal-atom vacancies in crystals of composition $TiC_{0.94}$ and $TiN_{0.99}$, and none were detected in our experiments. An increase in the X-vacancy concentration would have to occur to compensate for any Ti vacancies, and this would enhance the Ti-atom static displacements. Another possible effect could be a displacement of the nonmetal atoms, but this has not been observed either. X-ray powder-diffraction studies on TiC_{1-x} and the parent compounds ZrC_{1-x} and HfC_{1-x}, $0 \leq x \leq 0.5$ have shown[41] that the magnitude of the metal-atom displacements depend on composition, but the analysis is in terms of an isotropic attenuation factor due to static displacements, assumed to vanish at low concentrations (e.g., $TiC_{0.97}$). Our results clearly indicate that this approach is too simplistic. It gives a root-mean-

square displacement of only 0.033 Å for $TiC_{0.94}$.

An elastic diffuse neutron-scattering study on the more-carbon-deficient $TiC_{0.76}$ shows[42] that carbon-atom vacancies tend to avoid making themselves second neighbors and that the metal-carbon first-neighbor distances are shortened by about 0.03 Å, the metal atoms moving away from the C vacancies.

Assuming that the Ti atoms also move away from the C vacancies in $TiC_{0.94}$, our model consists of undistorted TiC_6 octahedra with Ti-C distances of 2.165 Å, and of TiC_5 square pyramids with an axial Ti-C distance of 2.068 Å and equatorial Ti-C distances of 2.167 Å.

E. Valence orbital population and charge transfer

Despite their close similarity in atomic constituents, crystal structure, and physical properties, titanium carbide and nitride differ significantly with respect to the population of their atomic orbitals, particularly with respect to the charge anisotropy in their metal $3d$ valence shell, measured here by the total number of electrons contributing to the nonsphericity of the $3d$-electron density, the $p(3d)_{\text{nonspherical}}$.

In the $TiC_{0.94}$, $[0.75(4)]e$ in the e_g and $[0.76(4)]e$ in the t_{2g} orbitals correspond to an excess of $[0.24(5)]e$ shared by two orbitals of e_g symmetry superposed on a spherical shell that contains $[1.27(6)]e$. In $TiN_{0.99}$, $[0.35(4)]e$ in the e_g and $[0.65(5)]e$ in the t_{2g} orbitals produce an excess of $[0.12(9)]e$ shared by three orbitals of t_{2g} symmetry on a spherical shell that contains $[0.88(11)]e$ (see Tables I and II).

The metal $4s$- and the nonmetal $2s$- and $2p$-orbital populations are less well defined than the $3d$ ones, primarily because the domain of reciprocal space where they scatter the most is poorly sampled owing to the small unit-cell dimensions and the Bravais-lattice type, and also because the domain includes exclusively strong reflections most severely affected by anisotropic extinction. Consequently, the net atomic charges bear substantial relative errors. Nevertheless, the refined orbital populations are chemically reasonable, $[0.4(4)]e$, $[3.1(4)]e$, and $[3.1(6)]e$ in the metal $4s$ and nonmetal $2s$ and $2p$ orbitals of the carbide and, respectively, $[1.1(4)]e$, $[1.8(6)]e$, and $[5.1(7)]e$ for the nitride. (The poorest values are within three estimated standard deviations of the maximum physically meaningful value.) This leads to a total electron count per atomic species of $20.0e$ for Ti and $8.2e$ for C in the carbide, and $20.1e$ for Ti and $8.9e$ for N in the nitride, due account being taken of nonstoichiometry. This corresponds to a charge transfer of $[2.1(4)]e$ from the metal to the nonmetal in $TiC_{0.94}$ and of $[1.9(4)]e$ in $TiN_{0.99}$, these values being similar to the one found in CaO,[43] isoelectronic isostructural to TiC.

Numerically different values (although the differences are statistically insignificant) were obtained from the refinements on the extensive data sets, $[1.4(5)]e$ for the carbide and $[1.3(5)]e$ for the nitride, but this is a direct consequence of including a large number of accurately measured, equivalent, low-order reflections in order to obtain a proper refinement of the numerous anisotropic extinction parameters, together with the atomic parameters, while in the subsequent refinement on the extinction-corrected, unique data sets, these very same reflections are relatively downweighted since they show larger external deviations upon averaging than high-order reflections. Altogether, this emphasizes the limitations of the present method of determining the electron-density distribution.

F. Orbital expansion-contraction

The most important changes in the radial charge distribution, as compared to that of the reference free atoms, occur with the metal $3d$ orbitals. Both the e_g and the t_{2g} sets of orbitals contract by about the same amount in $TiC_{0.94}$, $\kappa_{e_g}=1.47(7)$ and $\kappa_{t_{2g}}=1.77(8)$, and in $TiN_{0.99}$, $\kappa_{e_g}=1.42(12)$ and $\kappa_{t_{2g}}=1.40(8)$, as a result of the metal atoms bearing similar net positive charges. In this respect, $4s$ orbitals behave anomalously in showing a slight expansion, $\kappa_{4s}\sim 0.9(1)$. As for the negatively charge nonmetal atoms, the $2s$ orbitals expand in both compounds, $\kappa_{2s}\sim 0.8(1)$, while the $2p$ orbitals remain practically unchanged in the nitride, $\kappa_{2p}=0.96(6)$, but contract in the carbide, $\kappa_{2p}=1.23(7)$. The somewhat uneven results in the carbide are not surprising in the presence of a strong perturbation due to static displacements.

It is worth noting that the κ values obtained here follow a similar trend to that observed in a model fit to the theoretical structure factors discussed in the following article,[4] which shows, in particular, that κ_{e_g} might differ from $\kappa_{t_{2g}}$.

G. Valence-electron density

Static valence-electron density maps have been calculated for hypothetical stoichiometric, defect-free crystals of TiC and TiN. The maps were obtained by Fourier summation using as coefficients the contributions of the valence orbitals $(2s,2p,4s,3d)$ to the structure factors, computed from the occupancies, and scaled according to composition (i.e., $\not{\kappa}_M=1$ in the equation for charge neutrality) and the radial expansion-contraction parameters derived from the sophisticated model refinement "no ext." Thus effects due to statically displaced metal atoms, thermal motion, and nonstoichiometry should be absent, and these maps are directly comparable to the maps obtained from theoretical band-structure calculations. $(1\bar{1}0)$ sections are depicted in Figs. 9 and 10 for TiC and TiN, respectively. They represent the superposition of strictly spherically symmetric nonmetal atoms and of deformed metal atoms with a maximum electron density at the nuclear position of $7.5e$ Å^{-3} and $3.2e$ Å^{-3} for TiC, and $6.0e$ Å^{-3} and $1.3e$ Å^{-3} for TiN, respectively.

Since the number of electrons giving rise to charge anisotropy around the Ti atoms is small compared to the total number of valence electrons, only a small distortion from spherical symmetry is observed—in the form of six humps pointing along the [100] direction in TiC, with a maximum density of $4.0e$ Å^{-3} at 0.17 Å from the nucleus, and of eight humps pointing along the [111] direction in TiN, with maximum density of $1.8e$ Å^{-3} at 0.21 Å from the nucleus.

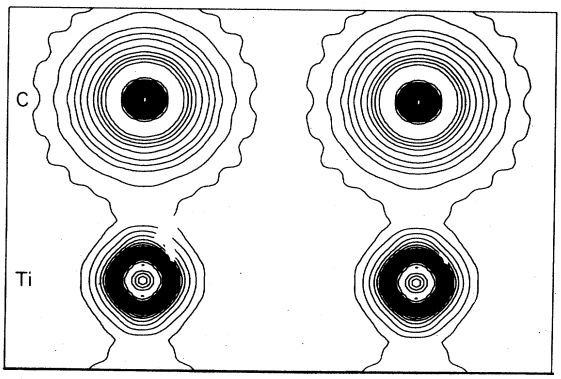

FIG. 9. Valence-electron density in the $(1\bar{1}0)$ plane of TiC for a hypothetical static, defect-free structure derived from the parameters of the refinement "no ext." Specifications and contours as in Fig. 1.

H. Bonding

Formally, our model does not allow for the possible occurrence of a cloud of electron density in the bonds, the traditional fingerprint of covalent bonds. However, it can be inferred from the respective residual maps that this type of buildup of charge density is small, if not absent, in both TiC and TiN. This renders the interpretation of our results in terms of chemical bonding the more speculative and qualitative.

Although the analysis of the TiC and TiN structures in terms of deformed atoms produces a satisfactory model of the electron density features, the fact that the orbital populations obtained, which are similar to a Mulliken partitioning, bear large relative errors puts a limitation on the description of the bonding. It is worth noting here that when refined against theoretical structure factors obtained from band-structure calculations,[4] our model leads to relative estimated errors of about 10% for the s- and p-orbital populations, 6% for the d ones, and 4% for the expansion-contraction coefficients, an indication of the ultimate limits of the method. It appears that an ionic, valence-bond-type description is well suited in this context.

A transfer of about $2e$ from the metal $4s$ and $3d$ orbitals to the nonmetal $2p$ orbitals, the $2s$ being filled, means that ionicity is important, although covalent bonding between atoms of different electronegativity can also lead to a large charge transfer. Then, the nonmetal $2p$ orbitals, which contain about $4.2e$ in TiC (i.e., assuming that the $1.07e$ excess in the $2s$ orbitals effectively belongs to the $2p$ orbitals) versus $4.9e$ in TiN, in agreement with the differences of electronegativity, can participate in covalent bonding with the metal e_g orbitals, which contain $0.75e$ in TiC versus $0.35e$ in TiN. On the other hand, the metal t_{2g} orbitals involve an equivalent number of electrons in TiC and TiN, $0.75e$ versus $0.65e$.

These features suggest that the metal-to-metal bonding is similar in both TiC and TiN, while the metal-to-nonmetal bonding is greater in TiC than in TiN. In any case, the $3d$ valence electrons behave as if mostly localized on the metal, and the valence-electron density goes through a minimum of $0.2e$ Å^{-3} along the M—X direction and through a minimum of $0.1e$ Å^{-3} along the diagonal M—M or X—X directions, hence giving a picture far different from the traditional one expected for the strong covalent bonds suggested by the properties of these compounds.

After completion of this paper, the results of three studies[44–46] along the same lines have been drawn to our attention. In the first two studies[44,45] the authors treat the atomic static displacements (in $TiC_{0.967}$) from the charge distribution (in $TiC_{0.96}$) separately. In the third study,[46] static displacements of 0.125(5) Å for the Nb atoms in NbC_{1-x} crystals $(0.05 \leq x \leq 0.12)$ were derived from an analysis of Debye-Waller factors.

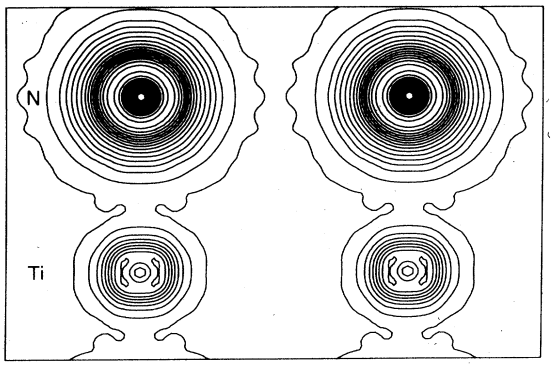

FIG. 10. Valence-electron density in the $(1\bar{1}0)$ plane of TiN. Same specifications as in Fig. 9, with $0 \leq s \leq 1.612$ Å^{-1}.

ACKNOWLEDGMENTS

We thank Dr. C. Politis, Kernforschungszentrum Karlsruhe, for supplying well-characterized single crystals of TiC and TiN. This work was supported by the Swiss National Science Foundation under Contract Nos. 2.246-0.79 and 2.404-0.82.

APPENDIX: SEPARATION OF d-ELECTRON ANISOTROPY AND STATIC ATOMIC DISPLACEMENTS

In reciprocal space, nonspherical effects in the electron density in cubic crystals can be studied most conveniently from their contribution to the differences between structure factors of paired reflections:

$$\Delta F_p = |F(h_1k_1l_1)| - |F(h_2k_2l_2)| ,$$

with

$$h_1^2+k_1^2+l_1^2 = h_2^2+k_2^2+l_2^2 .$$

For $TiC_{0.94}$ and $TiN_{0.99}$, the contributions to ΔF_p of charge asphericity, ΔF_{CA}, of small atomic static displacements along $\langle 100 \rangle$, ΔF_{SD}, and of anisotropic anharmonic thermal motion,[26] ΔF_{AM}, assumed to be independent of each other and due to the metal atoms only, may be expressed in terms of the same geometrical factor,

$$G = \frac{h_1^4+k_1^4+l_1^4}{(h_1^2+k_1^2+l_1^2)^2} - \frac{h_2^4+k_2^4+l_2^4}{(h_2^2+k_2^2+l_2^2)^2} ,$$

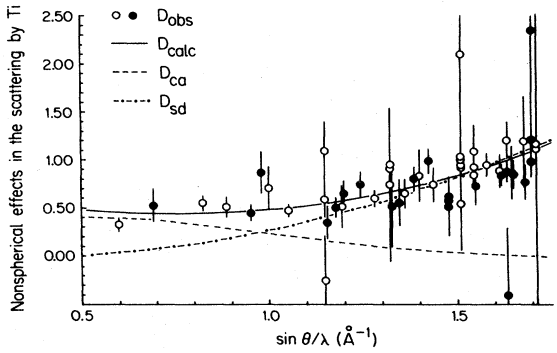

FIG. 11. Separation of nonspherical effects in $TiC_{0.94}$. Solid (open) circles denote even (odd) hkl indices. $3d$ contribution, — — —; static displacements, —·—·—·.

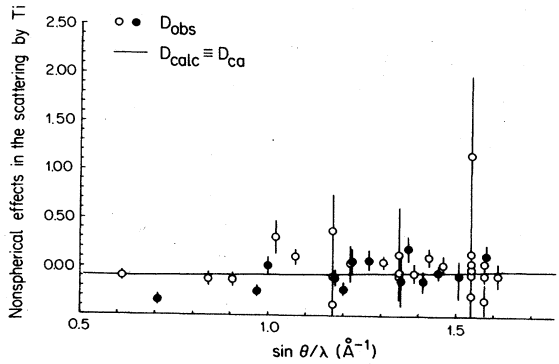

FIG. 12. Separation of nonspherical effects in $TiN_{0.99}$. Solid (open) circles denote even (odd) hkl indices.

provided the necessary truncated series expansions are applied to the structure-factor equation given in Sec. III B. The various symbols used are p, the population parameters; $\langle j_L(|s|)\rangle_{nl}$, the theoretical form factors; κ, the radial contraction parameters of the e_g and t_{2g} orbitals, respectively; $1-p_X$, the site-occupancy parameters and x_D, the fractional coordinate of the displaced metal atoms; $f_M(s)$, the relevant atomic scattering factor; a, the cell dimension; k_B, Boltzmann's constant; T, the absolute temperature; α, the potential parameter and δ, a parameter which determines the magnitude of the anharmonic, anisotropic contribution; and $s=(\sin\theta)/\lambda$.

For the sake of clarity, $h_1k_1l_1$ is taken as the vector closest to a [100] direction and the following quantities are defined:

$$D_{\mathrm{CA}}=G^{-1}\Delta F_{\mathrm{CA}}=\tfrac{20}{2}[\,\tfrac{3}{2}p_{e_g}\langle j_4(s/\kappa_{e_g})\rangle_{3d} - p_{t_{2g}}\langle j_4(s/\kappa_{t_{2g}})\rangle_{3d}]\,,$$

$$D_{\mathrm{SD}}=G^{-1}\Delta F_{\mathrm{SD}}=\tfrac{256}{3}\pi^4a^4(1-p_x)x_D^4f_M(s)[(\sin\theta)/\lambda]^4\,,$$

$$D_{\mathrm{AM}}=G^{-1}\Delta F_{\mathrm{AM}} =1024\pi^4(-\delta/\alpha^4)(k_BT)^3f_M(s)[(\sin\theta)/\lambda]^4\,,$$

which can be compared with the experimental values corrected for the effects of isotropic thermal motion:

$$D_{\mathrm{obs}}=G^{-1}[\,|F_0(h_1k_1l_1)|-|F_0(h_2k_2l_2)|\,]\times\exp\{8\pi^2\langle u^2\rangle[(\sin\theta)/\lambda]^2\}\,.$$

Figures 11 and 12 show scatter plots of D_{obs} as a function of $(\sin\theta)/\lambda$ for $TiC_{0.94}$ and $TiN_{0.99}$.

The contribution of charge asphericity to D_{obs} depends both on the form factor $\langle j_4\rangle_{3d}$ [and should therefore decrease monotonously past a value of 0.5 Å^{-1} in $(\sin\theta)/\lambda$], and on the ratio $p_{t_{2g}}/p_{e_g}$ (i.e., equation for D_{CA}, if $\kappa=1$). A ratio of less than 3/2 implies that the valence d electrons are predominantly of an e_g type, as verified in $TiC_{0.94}$, and, conversely, a ratio larger than 3/2 means that the t_{2g} type is predominant, as seen in $TiN_{0.99}$. Roughly estimated ratios are 1 in the former and 2 in the latter compound.

The contribution of atomic static displacements along $\langle 100\rangle$ to D_{obs} varies as $f_M(s)[(\sin\theta)/\lambda]^4$ (i.e., the equation for D_{SD}). Hence, the dramatic increase of D_{obs} in $TiC_{0.94}$ for $(\sin\theta)/\lambda<1.1$ Å^{-1} confirms the interpretation of the difference map and gives a tentative estimate of the displacements of 0.10 Å from the mean Ti-atom position. No such effect appears to be present in $TiN_{0.99}$. The contribution of anisotropic anharmonic thermal motion has the same dependence on $(\sin\theta)/\lambda$ as that of the atomic static displacements considered here (i.e., the equation for D_{AM}; note that displacements along $\langle 110\rangle$ and $\langle 111\rangle$ also have a similar functionality), but it is expected to have a smaller amplitude and therefore will be neglected in the following analysis. This effect does not seem to be present in $TiN_{0.99}$ either.

[1] L. E. Toth, *Transition Metal Carbides and Nitrides,* Vol. 7 of *Refractory Materials* (Academic, New York, 1971).

[2] A Neckel, Int. J. Quantum Chem. XXIII, 1317 (1983).

[3] *Electron Distributions and the Chemical Bond,* edited by P. Coppens and M. B. Hall (Plenum, New York, 1982).

[4] P. Blaha, J. Redinger, and K. Schwarz, following paper [Phys. Rev. B 31, 2316 (1984)].

[5] P. Blaha and K. Schwarz, Int. J. Quantum Chem. XXIII, 1535 (1983).

[6] A. Neckel, P. Rastl, R. Eibler, P. Weinberger, and K. Schwarz, J. Phys. C 9, 579 (1976).

[7] C. Politis (private communication).

[8] C. Politis, Th. Wolf, and H. Schneider, *Proceedings of the 7th International Conference on Chemical Vapor Deposition* (Electrochemical Society, Princeton, N.J., 1979), Vol. 79, pp. 289–299.

[9] *International Tables for X-ray Crystallography* (Kynoch, Birmingham, 1974), Vol. IV.

[10] E. K. Storms, *The Refractory Carbides* (Academic, New York, 1967), p. 8.

[11] S. Nagakura, T. Kusunoki, F. Kakimoto, and Y. Hirotsu, J. Appl. Crystallogr. 8, 65 (1975).

[12] A. Dunand and H. D. Flack, Acta Crystallogr. Sect. A 37, C315 (1981).

[13] T. Fukamachi, Jpn. J. Appl. Phys. 8, 851 (1969).

[14] E. D. Stevens, Acta Crystallogr. Sec. A 30, 184 (1974).

[15] *Landolt-Börnstein* (Springer, Berlin, 1979), Group III, Vol. 11.

[16] R. H. Blessing, P. Coppens, and P. Becker, J. Appl. Crystallogr. 7, 488 (1974).

[17] M. S. Lehmann and F. K. Larsen, Acta Crystallogr. Sect. A

30, 580 (1974).
[18]M. S. Lehmann, J. Appl. Crystallogr. **8**, 619 (1975).
[19]H. D. Flack and M. G. Vincent, Acta Crystallogr. Sect. A **34**, 489 (1978).
[20]Unless stated otherwise, all computations were performed with the XRAY'76 system: J. M. Stewart, P. A. Machin, C. W. Dickinson, H. L. Ammon, H. Heck, and H. Flack, Technical Report No. TR-446, Computer Science Center, University of Maryland, College Park, Maryland (1976).
[21]P. J. Becker and P. Coppens, Acta Crystallogr. Sect. A **30**, 129 (1974).
[22]P. J. Becker and P. Coppens, Acta Crystallogr. Sect. A **30**, 148 (1974).
[23]P. J. Becker and P. Coppens, Acta Crystallogr. Sect. A **31**, 417 (1975).
[24]W. H. Zachariasen, Acta Crystallogr. **23**, 558 (1967).
[25]H. D. Flack, M. G. Vincent, and J. A. Vincent, Acta Crystallogr. Sect. A **36**, 495 (1980).
[26]B. T. M. Willis and A. W. Pryor, *Thermal Vibrations in Crystallography* (Cambridge University Press, Cambridge, 1975), pp. 150—151.
[27]R. McWeeny, Acta Crystallogr. **4**, 513 (1951).
[28]A. J. Freeman, Acta Crystallogr. **12**, 261 (1959).
[29]R. J. Weiss and A. J. Freeman, J. Phys. Chem. Solids **10**, 147 (1959).
[30]B. Dawson, Acta Crystallogr. **17**, 990 (1964).
[31]B. Dawson, Acta Crystallogr. **17**, 997 (1964).
[32]T. Fukamachi, Tech. Rep. Inst. Solid State Phys. Univ. Tokyo, Ser. B **12**, 1 (1971).
[33]P. Coppens, Isr. J. Chem. **16**, 159 (1977).
[34]V. Moisy-Maurice, Centre d'Etudes Nucléaires Saclay (Gif-sur-Yvette) Report No. CEA-R-5127 (1981).
[35]F. R. Thornley and R. J. Nelmes, Acta Crystallogr. Sect. A **30**, 748 (1974).
[36]H. D. Flack and A. Dunand (unpublished).
[37]Y. Le Page and E. J. Gabe, J. Appl. Crystallogr. **11**, 254 (1978).
[38]H. D. Flack, program MARVEL (unpublished).
[39]Numerical Algorithms Group, NAG Library (NAG Central Office, Oxford, United Kingdom, 1981).
[40]F. K. Larsen (private communication).
[41]I. I. Timofeeva and L. A. Klochkov, in *Refractory Carbides*, edited by G. V. Samsonov (Consultants Bureau, New York, 1974), pp. 239—245.
[42]V. Moisy-Maurice, C. H. de Novion, A. N. Christensen, and W. Just, Solid State Commun. **39**, 661 (1981).
[43]G. Vidal-Valat, J. P. Vidal, and K. Kurki-Suonio, Acta Crystallogr. Sect. A **34**, 594 (1978).
[44]P. Čapková, R. Kužel, and J. Šedivý, Phys. Status Solidi A **76**, 383 (1983).
[45]V. Valvoda and P. Čapková, Phys. Status Solidi A **81**, 203 (1984).
[46]T. H. Metzger, J. Peisl, and R. Kaufmann, J. Phys. F **13**, 1103 (1983).